

The influence of nanogel amphiphilicity on dermal delivery: Balancing surface hydrophobicity and network rigidity

Alexandra Gruber,¹ Aaroh Anand Joshi,² Patrick Graff,² José Luis Cuéllar-Camacho,³ Sarah Hedtrich,^{2,4} Daniel Klinger^{1}*

¹Institute of Pharmacy (Pharmaceutical Chemistry), Freie Universität Berlin, Königin-Luise-Straße 2-4, 14195 Berlin, Germany

² Institute of Pharmacy (Pharmacology and Toxicology), Freie Universität Berlin, Königin-Luise-Straße 2-4, 14195 Berlin, Germany

³Institute of Chemistry and Biochemistry, Freie Universität Berlin, Takustraße 3, 14195 Berlin, Germany

⁴Faculty of Pharmaceutical Sciences, University of British Columbia, Wesbrook Mall, V6T1Z3 Vancouver, Canada

E-mail: daniel.klinger@fu-berlin.de

Table of Contents

1. Monitoring the conversion of PPFMA network to amphiphilic networks.....	2
2. Transmission electron microscopy.....	4
3. Particle characterization by angle-dependent dynamic light scattering.....	5
4. Atomic Force Microscopy.....	7
5. Dermal delivery of Nile red loaded and FITC functionalized NGs.....	15

1. Monitoring the conversion of PFPMA network to amphiphilic networks

The successful conversion of the pentafluorophenyl esters (PFP) (1778 cm^{-1}) to the respective amides (1662 cm^{-1}) was followed by attenuated total reflection Fourier-transform infrared spectroscopy (ATR-FTIR) on freeze-dried NGs (Figure S 1). Quantitative conversion of the PFP ester groups was demonstrated *via* ^{19}F NMR exemplarily for CHOLA-20 NGs (Figure S 2).

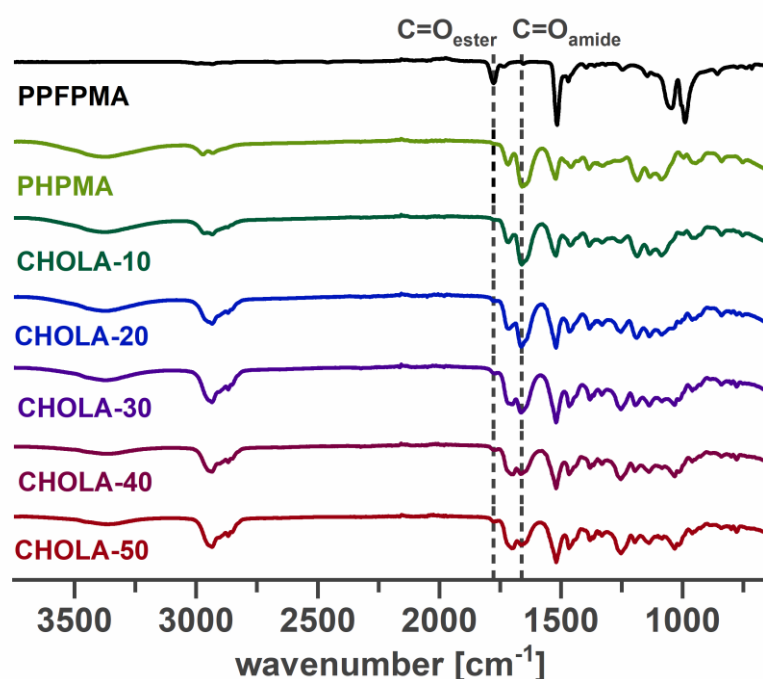


Figure S 1. Successful network functionalization of the NGs is demonstrated by the disappearance of the reactive PFP ester bands and the simultaneous appearance of the amide bands in ATR-FTIR spectra.

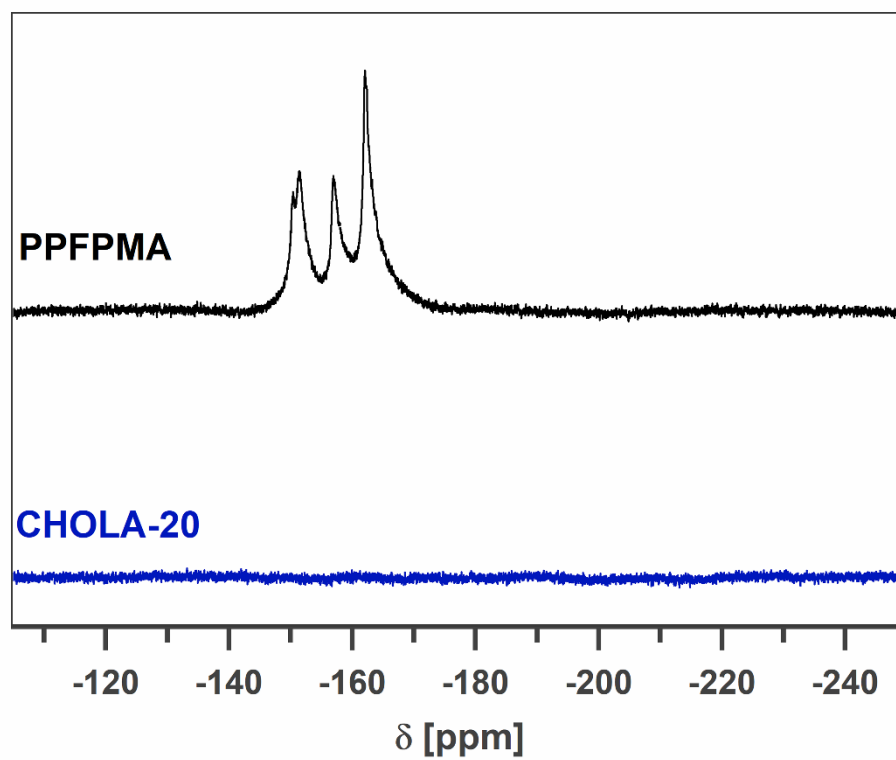


Figure S 2. Successful network functionalization is demonstrated by the disappearance of the PFP ester peaks in ^{19}F NMR spectra, exemplarily shown for CHOLA-20 NGs.

2. Transmission Electron microscopy

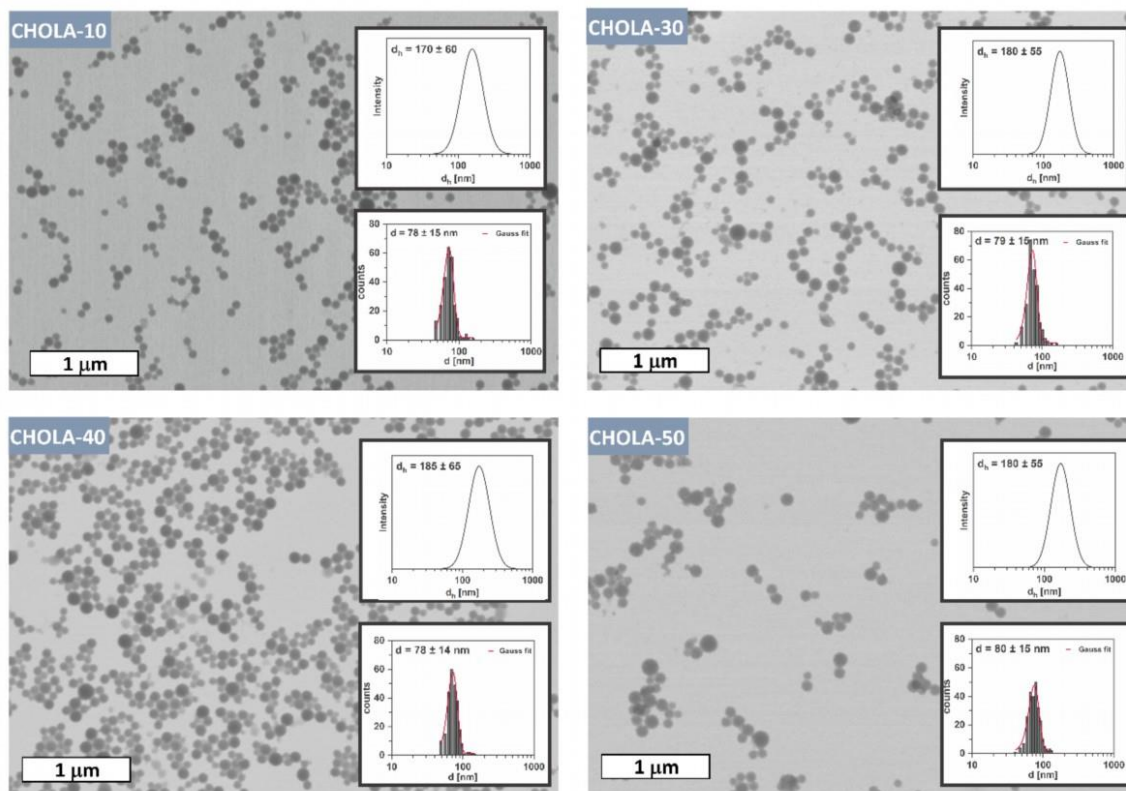


Figure S 3. Post-functionalization of reactive precursor particles results in well-defined NGs with different hydrophobicity but similar colloidal features as size and size distribution as demonstrated by TEM images and their respective statistical evaluation of the NG sizes in their dried state (bottom inset) and DLS measurements at an angle of 90° (top inset).

3. Particle characterization by angle-dependent dynamic light scattering

Particle size distributions were determined by dynamic light scattering, performed on a Nicomp Nano Z3000 (Particle Sizing Systems, Port Richey, United States of America). The measurements were carried out at 23 °C on diluted dispersions in water. Angle-dependent measurements were carried out at scattering angles of 70°, 80°, 90°, 100° and 110°. The apparent diffusion coefficient D_{app} was provided by the Nicomp Nano Z3000 by cumulant analysis of the autocorrelation function and plotted against the quadratic scattering vector q^2 . By extrapolation of the plotted data to the y-intercept, the z-average diffusion coefficient D_s was obtained (exemplary for PHPMA NGs Figure S 4). D_s was used to calculate the hydrodynamic diameter of the nanogels.

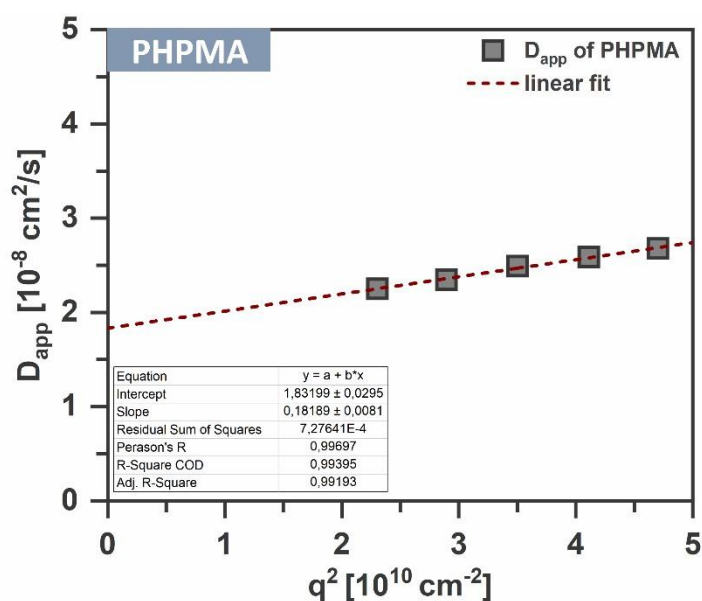


Figure S 4. Extrapolation to the y-intercept of the apparent diffusion coefficient D_{app} plotted against the quadratic scattering vectors gives access to the Z-average diffusion coefficient. Representative shown for PHPMA NGs.

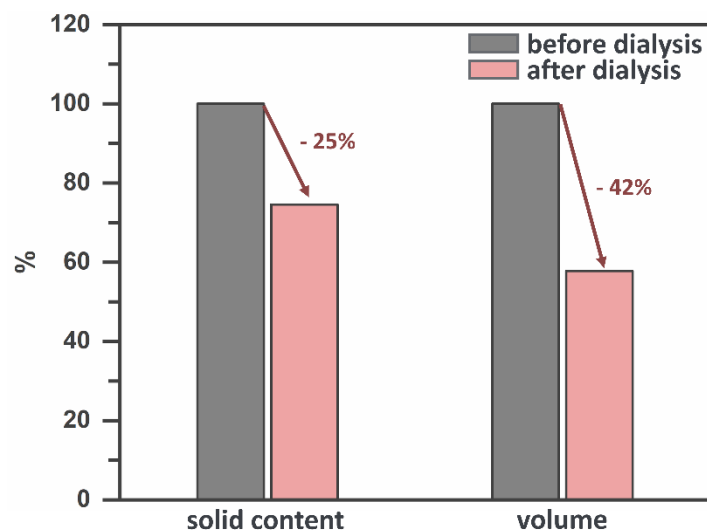


Figure S 5. Dialysis of PPFMA precursor particles results in a volume decrease due to removal of unreacted monomer which correlates well with the solid content of the particles after freeze drying.

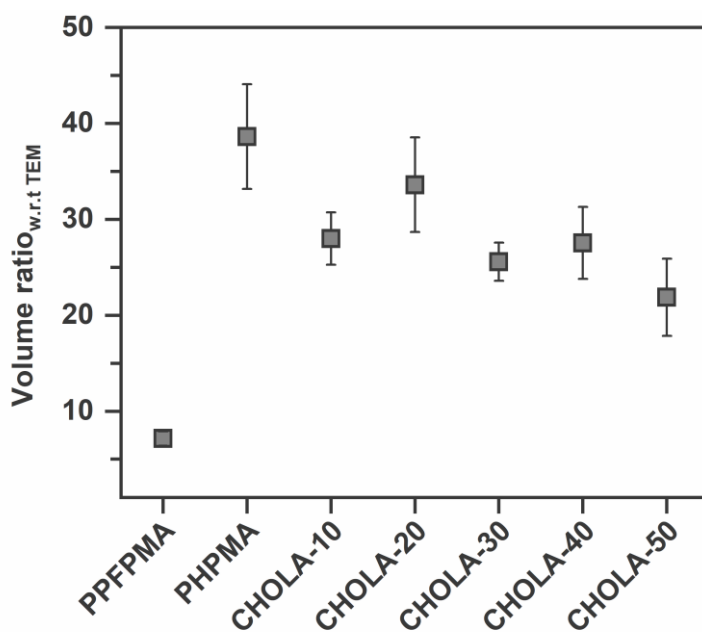


Figure S 6. Volume ratio of NGs show that the hydrophilic NGs swell more than the amphiphilic ones and the respective precursor particles. Volume ratio of hydrated NGs with respect to their dried state was determined by dividing the volume of the particles determined *via* angle dependent DLS measurements by the volume of the particles in their dried state determined *via* the evaluation of TEM images. Error bars represent the standard deviation of 6 measurements.

4. Atomic force microscopy

Height AFM measurements in PeakForce mode

AFM measurements in PeakForce mode in a closed fluid cell enable the depiction of NGs with varying hydrophobicity in their water swollen state (Figure S 7). Furthermore, evaluation of cross section profiles of 20 NGs per samples gives an average height and width of the NGs (Table S1)

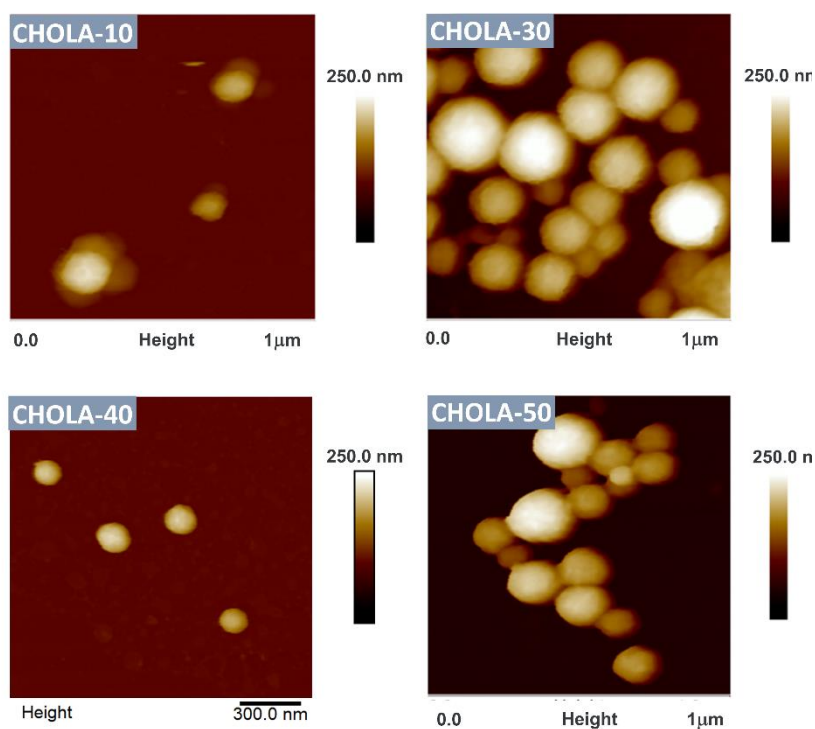


Figure S 7. Height AFM images obtained in PeakForce mode show well defined NGs of different hydrophobicity in their swollen state in Milli-Q water.

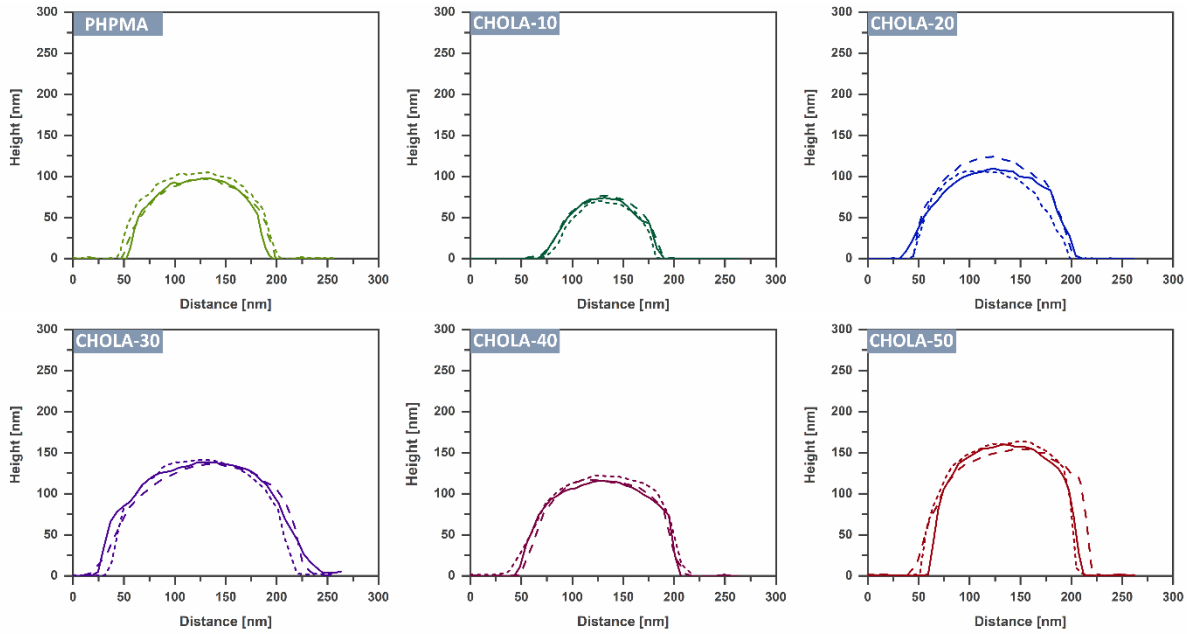


Figure S 8. Three individual cross section profiles of NGs of different amphiphilicity show comparable sizes.

Table S 1. Measured lateral and vertical dimensions of amphiphilic NGs using atomic force microscopy. Mean width and height are taken from measurements of cross section profiles of 20 single NGs as shown in figure 2d) of the main text.

Sample	Width (nm)	Height (nm)
PHPMA	164 ± 34	104 ± 24
CHOLA-10	118 ± 63	72 ± 20
CHOLA-20	154 ± 20	110 ± 16
CHOLA-30	238 ± 40	154 ± 26
CHOLA-40	172 ± 44	132 ± 22
CHOLA-50	172 ± 42	146 ± 26

Point Nanoindentations.

To investigate the materials properties of NGs we applied focalized compressions with sharp AFM tips model type SNL from Bruker with a nominal radius of $\sim 2\text{nm}$. Although in practice these AFM tips do not possess a perfect conical shape (front angle of 15° , back angle of 25° and side angle of 22.5°), and neither are exactly 2 nm in radius immediately after a sample has been imaged, the approximation of a conical indenter versus a flat elastic plane can still be made because their size and shape relative to NGs (radius $\sim 125\text{nm}$ from DLS in solution) is still substantial with a ratio of $R_{\text{tip}} / R_{\text{NG}} = 0.016$. In the model of contact of Sneddon, the force load F is related to the induced deformation δ by

$$F = \frac{2 E \tan(\alpha) \delta^2}{\pi(1 - \nu^2)}$$

Where E is the sample's Young's moduli, α is the half-opening angle spanned by the apex of the AFM tip (in the present case $\alpha = 20^\circ$), and ν is the Poisson ratio (in the present case a approximation of $\nu = 0.5$ is employed). It is worth to mention that for these novel composite materials we do not have any information regarding the Poisson ratio, and thus our estimation of the material properties accounts as a first approximation of their elasticity and mechanical stability. More detailed experimental studies are necessary to unveil and relate their mechanical properties as a function of their internal structure.

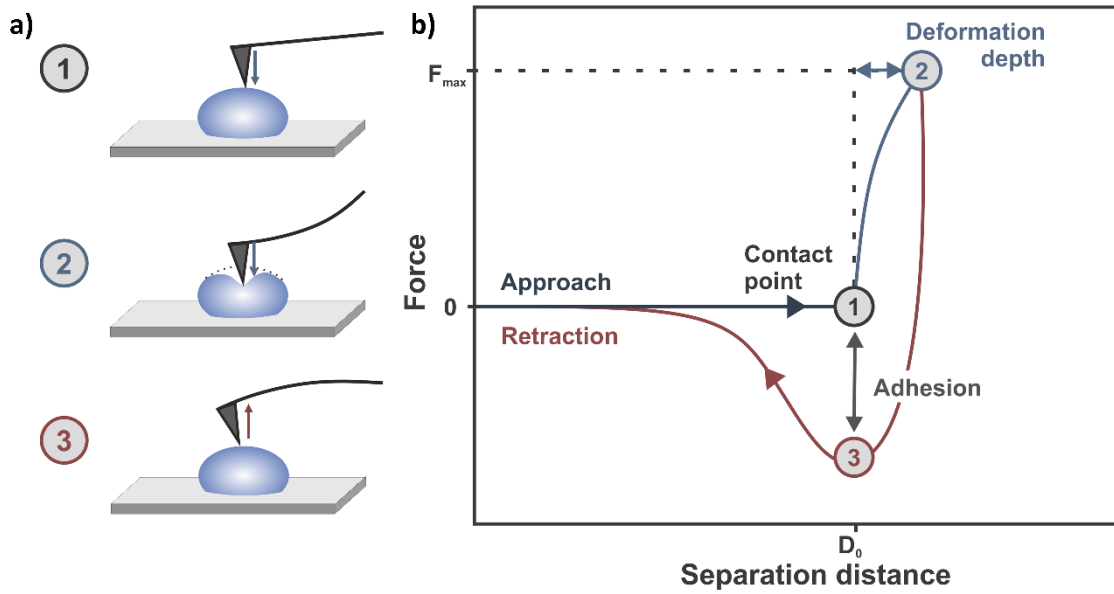


Figure S 9. Schematic (a) interaction of the AFM tip and a NG and (b) force-separation curve which gives access to physical parameters as height, deformation and adhesion. In 1, NG “height” is given by the vertical distance provided when the AFM tip contacts the NG surface with respect to the surrounding substrate. In 2, deformation is obtained as the vertical distance traveled by the tip from the point the AFM tip contacts the NG surface, until the point the AFM tip reaches the maximum force set point. And in 3 upon retraction, adhesion is obtained from the magnitude of cantilever’s deflection beyond its equilibrium position, which is followed by the release of the interaction between AFM tip and NG.

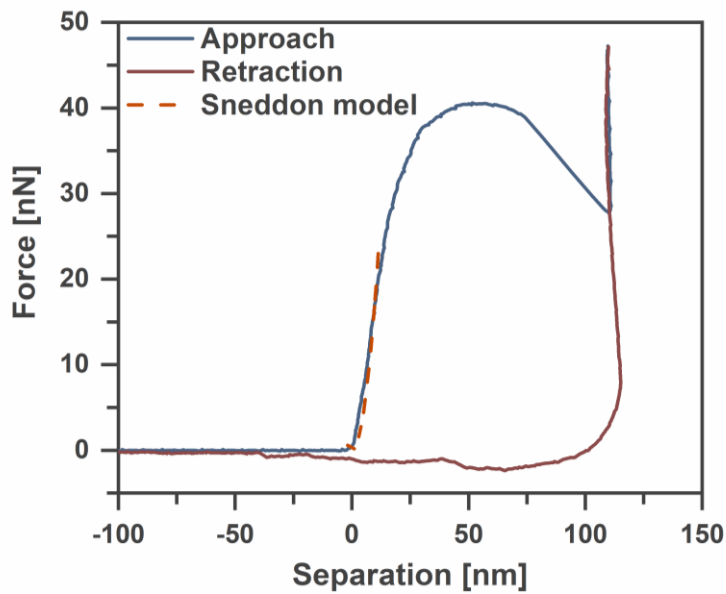


Figure S 10. Representative force-separation curve showing approach and retraction traces during indentation on a CHOLA-40 NG. According to the present geometry and relative size between AFM tip and nanogel at contact, the Sneddon model of contact is used to obtain a first estimate of the nanogel's Young's moduli. A fit to experimental data is taken following the point of contact, which is shown with a dashed red curve. Upon retraction, the red curve clearly shows a lack of material recovery or response, which might suggest that after crossing certain force threshold (fracture or failure point in blue curve at about 40 nN) irreversible structural damage has been permanently inflicted on the nanogel.

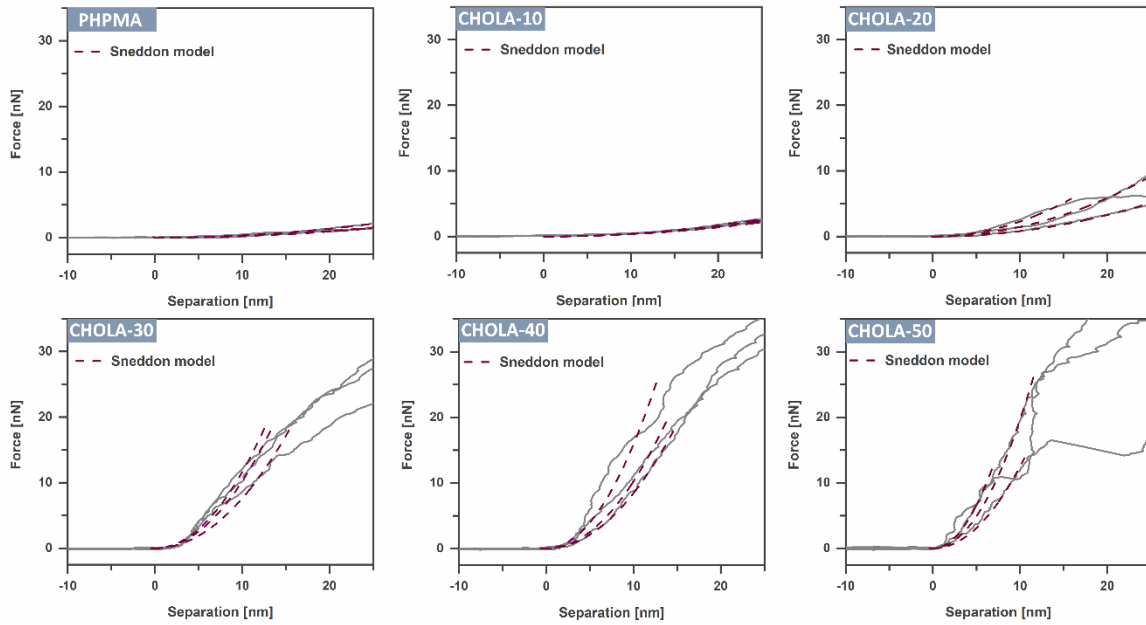


Figure S 11. Force separation curves obtained from nanoindentation for all NG functionalizations are shown for the first 25 nm to enable comparison. A fit to the Sneddon model is applied within the first 12 nm or 25 nm before fractures or irreversible damage is shown to occur in the curve.

AFM adhesion measurements (in PeakForce mode):

AFM measurements in PeakForce mode not only provides nanoscale resolution of surface topography, but it also enables simultaneous mapping of physical parameters. For this the AFM tip pushes the sample repeatedly with a predefined maximal force before retraction occurs in a reversible fashion. During retraction, the strength of adhesion can be measured as attractive interaction between the tip and the sample (Figure S9). Thus, mapping the adhesion forces can be used to measure differences in interaction of the AFM tip with the substrate and with the NGs. These differences in adhesion can be interpreted as measure of NG hydrophobicity. In Figure S 12 and S13 shows that an increasing CHOLA content resulted in a significant reduction of the adhesion differences between tip-substrate and tip-NG. This correlates with the surface hydrophobicity of the NGs and shows the anticipated trend that an increase in CHOLA groups not only lead to an increase in the internal but also on the surface hydrophobicity.

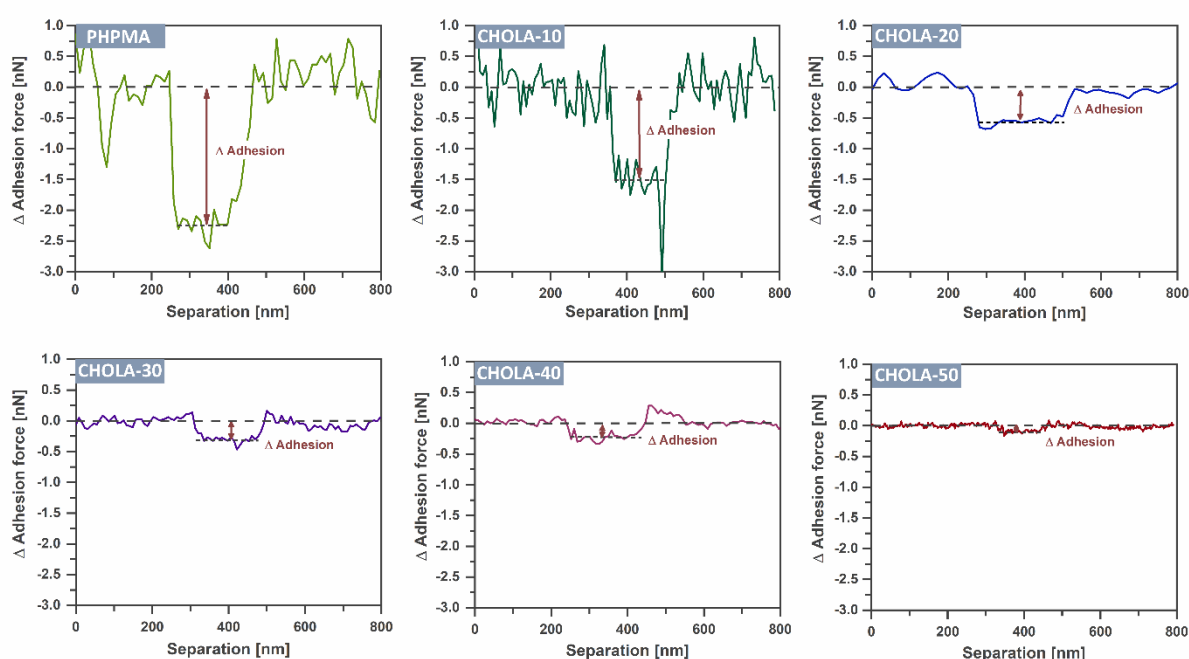


Figure S 12. Adhesion force measurements show that with increasing CHOLA content the surface hydrophobicity increases.

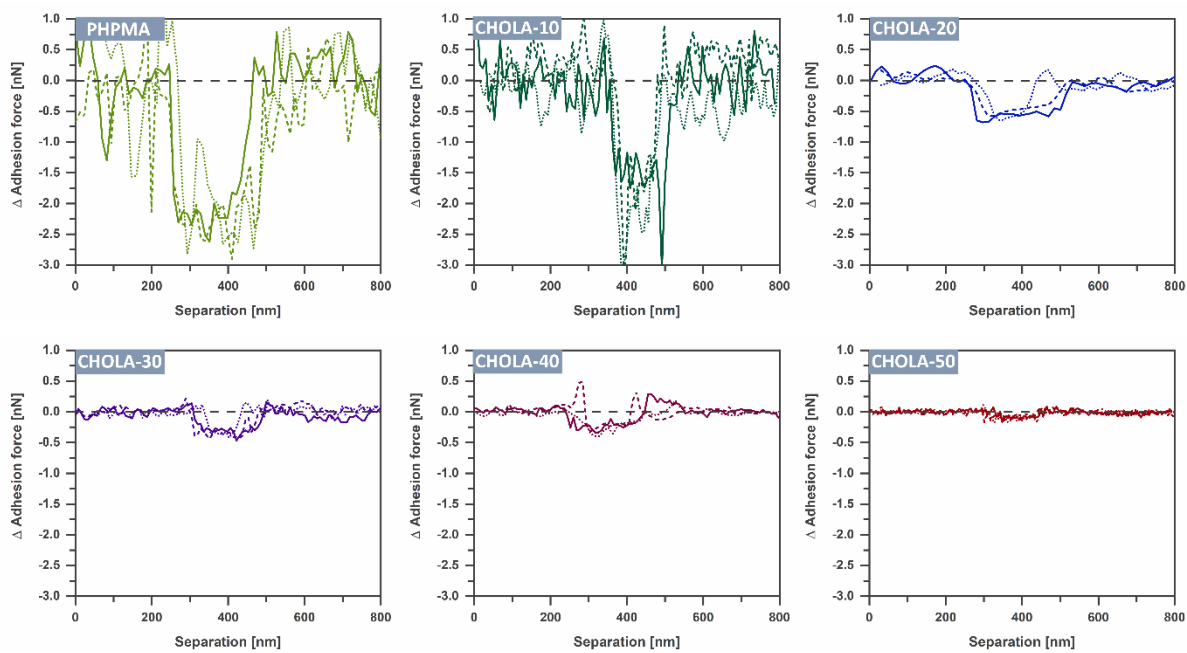


Figure S 13. Overlay of three individual adhesion force measurements of different NGs each CHOLA functionalization show reproducibility of the technique.

5. Dermal delivery of Nile red loaded and FITC functionalized NGs

Determination of Nile Red loading and FITC functionalization

To enable investigation on the influence of the surface hydrophobicity and mechanical properties of NGs with varying CHOLA content on their topical delivery efficiency, two main requirements needed to be fulfilled: First, the cargo as well as the NGs need to be traceable within the skin. Second, to ensure comparability and enable systematic studies the NGs need to be labelled equally and carry the same amount of traceable cargo.

As cargo we used NR, a hydrophobic, water-insoluble dye of bright fluorescence which is considered as model compound for corticosteroids due to its low molecular size and high hydrophobicity ($\log P$ 3.8). To ensure comparability, all NGs were loaded with the same amount of NR (0.3 wt-%) using the co-solvent method. The offered amount of NR was much lower than the maximum loading capacity determined for the most hydrophilic NGs in a previous study.¹ Thus, all NGs are able to fully encapsulate the provided NR. Quantification was achieved relative to a NR calibration curve (Figure S 14) confirming a NR loading of 0.3 wt-% for all NGs (Figure S 15). In order to track the NGs in the skin, FITC was covalently attached

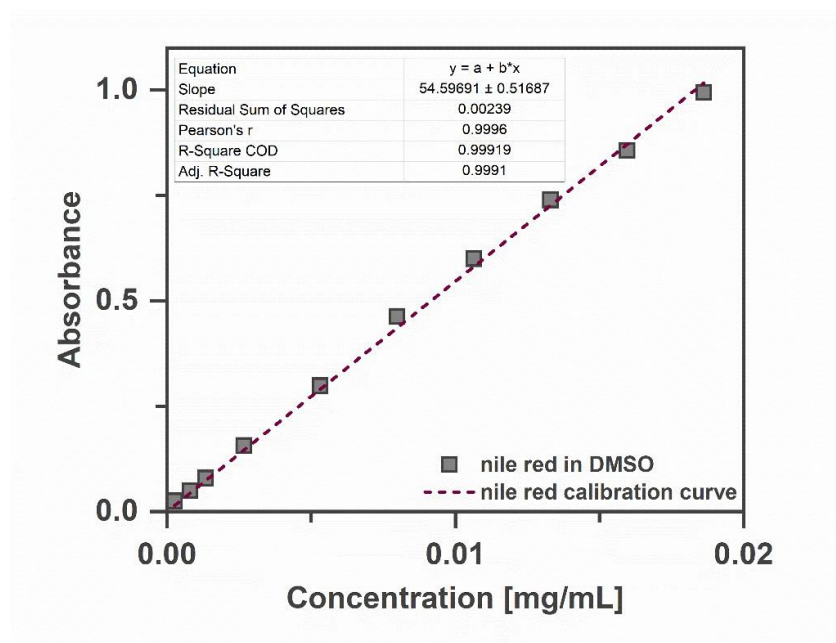


Figure S 14. Calibration curve of Nile red in DMSO at 552 nm.

to the NGs. Here we strongly benefit from our reactive precursor strategy. By introducing the FITC to the precursor particles before introducing the amphiphilicity, the fluorescence label is translated to the different NGs equally (Figure S 15).

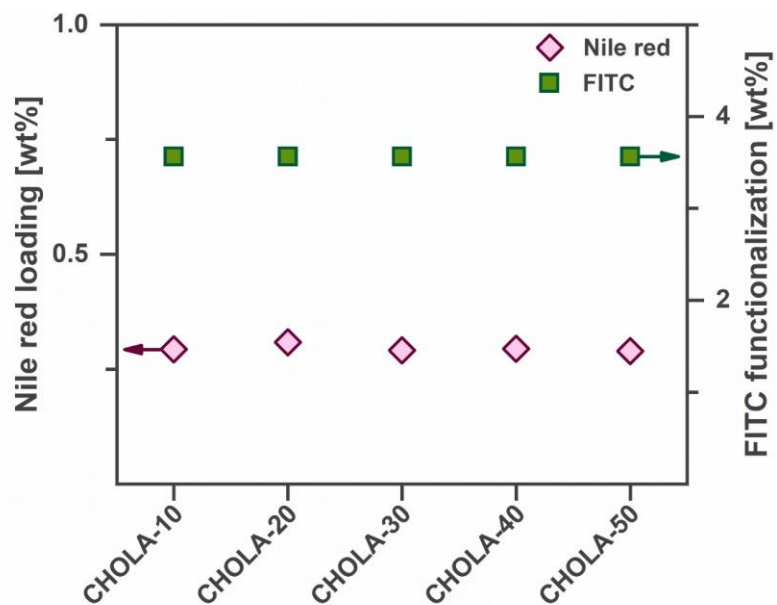


Figure S 15. Similar NR loading and identical FITC-functionalization for all NGs due to reactive precursor approach.

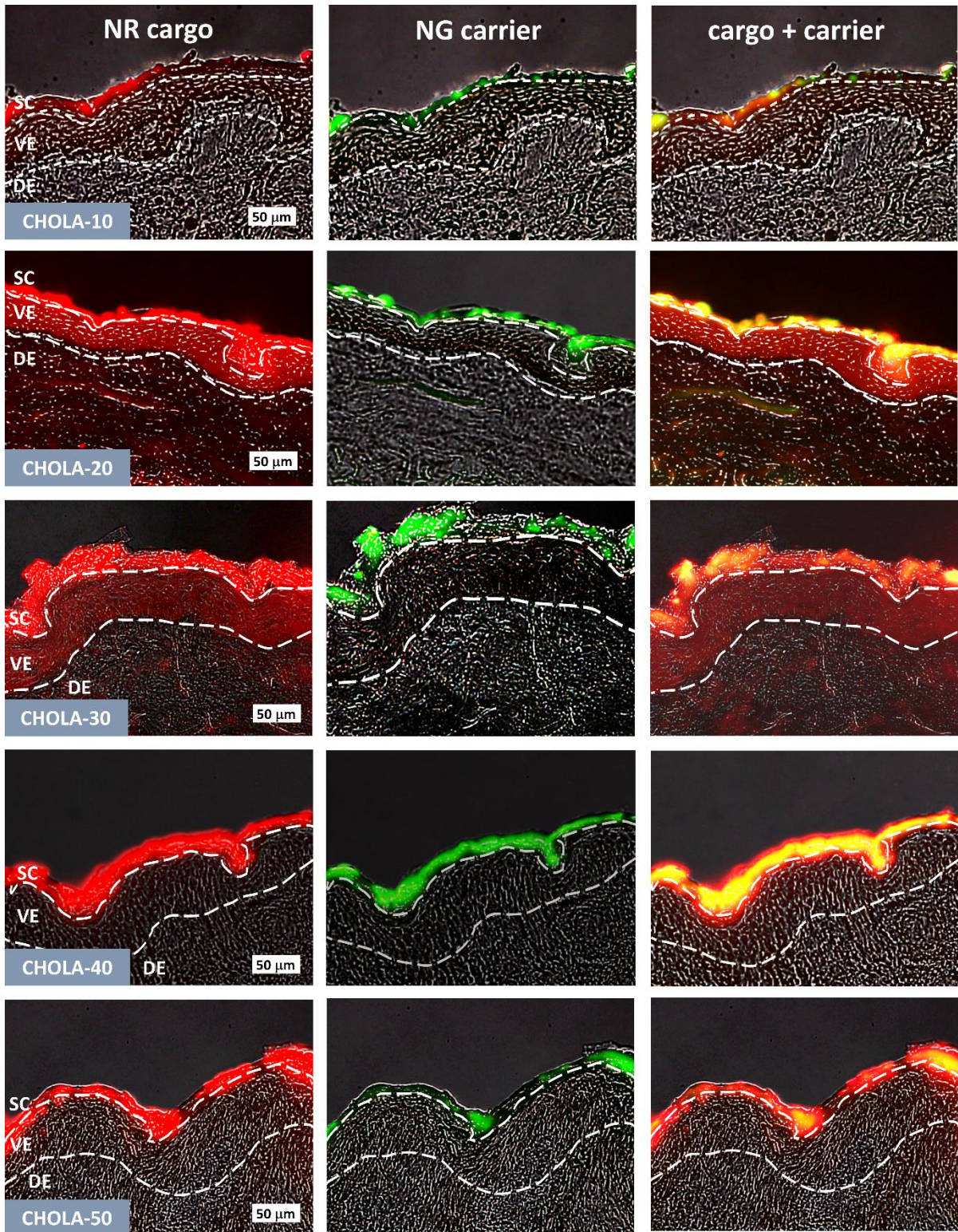


Figure S 16. CHOLA-20 and CHOLA-30 NGs show suitable network amphiphilicity to interact with the skin and release their cargo into deeper skin layers. Fluorescence images: NR channel left column, FITC channel middle column and merge of both right column. Dashed lines show the borders between the different skin layers and were determined from the respective bright field microscopy images.

1. A. Gruber, D. Işık, B. B. Fontanezi, C. Böttcher, M. Schäfer-Korting and D. Klinger, *Polym. Chem.*, 2018, **9**, 5572-5584